Food and Chemical Toxicology 209 (2026) 115924

Contents lists available at ScienceDirect

Food and Chemical Toxicology

journal homepage: www.elsevier.com/locate/foodchemtox

The cytotoxic effects of a single and combined exposure to the mycotoxins, deoxynivalenol and zearalenone, on a rat Leydig cell line (LC-540)

Mohammed I.A. Ibrahim [a,*], Antoinette V. Lensink [b], Christo J. Botha [a]

[a] Department of Paraclinical Sciences, Faculty of Veterinary Science, University of Pretoria, South Africa
[b] Electron Microscope Unit, Department of Anatomy and Physiology, Faculty of Veterinary Sciences, University of Pretoria, South Africa

ARTICLE INFO

Handling Editor: Professor Matthew Wright

Keywords:
Deoxynivalenol
Cytoskeletal disruption
Cytotoxicity
Leydig cells
Mitochondrial damage
Zearalenone

ABSTRACT

Deoxynivalenol (DON) and zearalenone (ZEA) are among the most prevalent mycotoxins synthesized by *Fusarium* species, with 60 % and 80 % prevalence in grains containing mycotoxins, respectively. These mycotoxins often co-contaminate feedstuffs and induce male reproductive toxicity. This study investigated *in vitro* cytotoxicity, the structure of selected cytoskeletal proteins, mitochondrial morphology, lysosomal activity, and ultrastructural changes associated with individual and combined DON and ZEA exposure in rat Leydig cells (LC-540). Deoxynivalenol (IC_{50}: 2.66, 0.50, and 0.44 μM) induced higher cytotoxicity than ZEA (IC_{50}: 117.0, 69.1, and 34.4 μM) after 24, 48, and 72 h, respectively. Combined DON + ZEA exposure revealed concentration- and time-dependent cytotoxic effects that were synergistic at low concentrations (0.125 + 10 μM), but additive or antagonistic at higher concentrations (2 + 30 and 5 + 50 μM). Microscopic analysis revealed both mycotoxins disrupted F-actin and β-tubulin, impaired mitochondrial morphology, and increased lysosomal acidification. Ultrastructurally, marked cellular alterations included mitochondrial damage, autophagosome formation, and apoptosis. The observed cytotoxicity, disruption of cytoskeletal proteins, and mitochondrial damage in the Leydig cells may play a role in clarifying the male reproductive toxicity induced by DON and ZEA or their co-exposure.

1. Introduction

Deoxynivalenol (DON) and zearalenone (ZEA) are two of the most common mycotoxins synthesized by *Fusarium* spp. (El-Sayed et al., 2022). These mycotoxins can contaminate food and feed, primarily grains (Sobrova et al., 2010; Zinedine et al., 2007), and may also occur as secondary contaminants in animal-derived products, particularly DON (Sobrova et al., 2010). Consequently, they can pose significant health risks to humans and livestock. It has been estimated that mycotoxins contaminate approximately 25 % of the world's agricultural products (World Health Organization & Food and Agriculture Organization of the United Nations, 2011). Eskola et al. (2020) reported that about 20 % of feed samples in 2010–2015 were contaminated by mycotoxins, with a 60 % and 80 % prevalence of DON and ZEA, respectively, in food grains. Pigs are especially susceptible when exposed to DON where acute exposure induces feed refusal and vomiting (Serviento et al., 2018). In animal models, chronic exposure to low DON doses results in loss of appetite, growth deficiency, immunotoxicity, as well as reproductive and developmental toxicities (Pestka, 2010). Zearalenone induces reproductive toxicity due to its potent estrogenic activity (Takemura et al., 2007) and disrupts male and female reproductive organ development (Li et al., 2021). In males decreased testosterone levels and impaired sperm quality and quantity have been reported (Yang et al., 2007b). Furthermore, it also causes immunotoxicity (Hueza et al., 2014), hepatotoxicity (Zhang et al., 2022), and genotoxicity (Ghedira-Chekir et al., 1999). Co-contamination of feedstuffs with DON and ZEA is common, thus, increasing the risk of reproductive toxicity in humans and animals (Thapa et al., 2021; Widodo et al., 2024).

The male reproductive toxicity of DON and ZEA has been documented in animal models. Damage to seminiferous tubules, impairment of spermatogenesis, disruption of the blood-testis barrier proteins, and testicular inflammation were reported in Kunming mice after being exposed to 1.2, 2.4, and 4.8 mg/kg DON for 28 days (Cao et al., 2020b). A reduction in sperm quality, including increased sperm abnormality and decreased sperm count, associated with diminished motility, has been observed in mice (Cao et al., 2020b; Hallaj Salahipour et al., 2019; Yang et al., 2019) and Sprague-Dawley rats (Sprando et al., 2005), exposed to DON. Exposure to 1, 2, and 4 mg/kg of ZEA for 28 days causes reproductive toxicity in male Wistar rats, specifically, dissociation of germinal cell epithelium, depletion of seminiferous tubules,

* Corresponding author.
E-mail address: u17372098@tuks.co.za (M.I.A. Ibrahim).

https://doi.org/10.1016/j.fct.2025.115924
Received 21 November 2025; Received in revised form 19 December 2025; Accepted 27 December 2025
Available online 30 December 2025

reduction of seminiferous tubule epithelial height, and interstitial edema (Adibnia et al., 2016). Furthermore, in adult mice (Kunming strain) ingesting high ZEA concentrations of 25, 50, and 75 mg/kg ZEA for 7 days, vacuoles were present in the germinal epithelium with decreased spermatogenic cells, live spermatozoa, serum testosterone, and sperm count (associated with increased sperm abnormality) (Yang et al., 2007a). The effect of co-exposure to DON and ZEA on the male reproductive system has also been investigated. A decrease in sperm quantity and survival rate, oxidative stress, and increased sperm abnormality were observed in mice exposed to 0.5 mg/kg DON and 1 mg/kg ZEA for 28 days (Cao et al., 2020a).

Leydig cells are interstitial testicular cells that play an important role in steroidogenesis, steroid hormone biosynthesis, and maintaining testicular spermatogenesis (Zirkin and Papadopoulos, 2018). In an effort to reduce, refine, and replace (3Rs) animals in experimentation (Yadav and Singh, 2021), Leydig cells have been used in *in vitro* mechanistic studies to evaluate reproductive toxicity caused by compounds (Lazzaretti et al., 2024; Li et al., 2024). Previous studies have examined the cytotoxic effects of mycotoxins on the Leydig cells of rodents (Savard et al., 2016; Yang et al., 2007a) and pigs (Sun et al., 2022). Both DON and ZEA induce oxidative stress, thereby inhibiting steroidogenesis; however, Savard et al. (2016) suggested that oxidative stress was not the main cause of steroidogenic failure.

Cytoskeletal proteins such as F-actin and β-tubulin are present in the Leydig cells and facilitate the transport of cholesterol from lipid droplets to mitochondria, an essential step in testosterone biosynthesis (Clark and Shay, 1981; Hall and Almahbobi, 1992; Sewer and Li, 2008; Wu and Zhang, 2022). Mitochondria contain essential steroidogenic enzymes, including cholesterol side-chain cleavage enzyme (CYP11A1) (Papadopoulos and Miller, 2012). Therefore, any alteration in the structure of cytoskeletal proteins or mitochondrial morphology may compromise steroidogenic activity. Based on previous studies various authors have concluded that exposure to DON and ZEA or their combinations disrupt testosterone synthesis and secretion (Sun et al., 2022; Yang et al., 2024; Zhao et al., 2021); however, their specific effects on cytoskeletal disruption and mitochondrial damage remain unknown. Accordingly, the aim of this study was to investigate the cytotoxic effects of exposure to DON, ZEA, and their combinations on selected cytoskeletal proteins, as well as the ultrastructure and mitochondrial morphology using a rat Leydig tumour cell line (LC-540).

2. Materials and methods

2.1. Chemicals and reagents

Cell culture reagents, including fetal bovine serum (FBS: Cat No. GI-12A) and penicillin/streptomycin solution 100x (Pen/Strep: Cat No. PS-B), were provided by Capricorn Scientific (Germany). Minimum Essential Medium Eagle (EMEM: Product No. M4655), phosphate-buffered saline (PBS: Product No. P4417), and Trypsin-EDTA solution 1x (Cat No. 59417c) were obtained from Sigma-Aldrich (USA). Mycotoxin standards deoxynivalenol (DON: CAS No. 51481-10-8, purity ≥98 %) and zearalenone (ZEA: CAS No. 17924-92-4, purity ≥99 %) were purchased from Sigma-Aldrich (USA). Solvents, including dimethyl sulfoxide (DMSO: CAS No. 67-68-5, purity ≥99.9 %) and ethanol (absolute), were procured from Sigma-Aldrich (USA). The Research Ethics Committee of the University of Pretoria approved this study (approval number REC133-22).

2.2. Cell culture and mycotoxin exposure studies

2.2.1. Cell culture

A Fischer rat testis Leydig tumour cell line (LC-540) obtained from the Japanese Collection of Research Bioresources Cell Bank (JCRB9064) was used to investigate the cytotoxic effects of individual and combined mycotoxin exposures. Cells were cultured in EMEM supplemented with 4 mM L-glutamine, 10 % FBS, and 1 % Pen/Strep (100 IU/mL). The cell culture was maintained in an incubator at 37 °C in a humidified 5 % CO_2 environment. For subculture, cells were seeded in 75 cm^2 culture flasks and passaged twice weekly. For cytotoxicity assays, LC-540 cells were seeded at appropriate densities in culture medium supplemented with 5 % FBS for 24 h prior to mycotoxin exposure to allow sufficient time for cell attachment and stabilization. The culture medium was changed as needed to maintain optimal growth conditions.

2.2.2. Mycotoxin preparation and treatment

Deoxynivalenol (DON) stock solution (3400 μM) was prepared by dissolving 2 mg DON (molecular weight 296.32 g/mol) in 2 mL ethanol. An intermediate dilution (50 μM) was prepared in 5 % FBS culture medium, followed by serial dilution to achieve final concentrations of 0.125, 0.25, 0.5, 1, 2, 4, 5, and 10 μM. A zearalenone (ZEA) stock solution (15705 μM) was prepared by dissolving 2 mg ZEA (molecular weight 318.364 g/mol) in 400 μL ethanol. Therefore, desired concentrations were prepared by serial dilution in 5 % FBS culture medium to achieve final concentrations of 10, 20, 30, 40, 50, 60, 80, and 100 μM. The concentration range was selected based on previous studies evaluating DON and ZEA cytotoxicity in Leydig cell lines, where IC_{50} values ranged from 0.25 to 12.3 μM for DON and 34–50 μM for ZEA after 24–48 h exposure, respectively (Eze et al., 2018; Savard et al., 2016). Moreover, higher concentrations were included to illustrate the dose-response profile. For combination studies, equal volumes of DON and ZEA concentrations were mixed to create combined exposure treatments. The mixing protocol resulted in a two-fold dilution of each mycotoxin, producing the following final concentrations for the DON + ZEA combination treatments: 0.0625 + 5, 0.125 + 10, 0.25 + 15, 0.5 + 20, 1 + 25, 2 + 30, 2.5 + 40, and 5 + 50 μM. Vehicle controls corresponding to ethanol concentrations in mycotoxin treatments (0.29 % for DON and 0.63 % for ZEA) and a positive control (0.01 % Triton X-100) were used.

In the additional studies, mycotoxin concentrations were determined using MTT and AlamarBlue® cytotoxicity assays. The 48 h was selected as the incubation period, and concentrations of 0.1 and 0.4 μM for DON, and 20 and 60 μM for ZEA were chosen to represent Sub-lethal and moderate cytotoxic doses. Cytotoxic effects were evaluated in three independent experiments with at least three replicates per treatment.

2.3. Cell viability studies

Mycotoxin-induced cytotoxicity was assessed using the MTT (Mosmann, 1983) and AlamarBlue® cell viability assays. Leydig cells were seeded in 96-well plates at 5×10^3 cells/well and 5×10^2 cells/well for MTT and AlamarBlue® assays, respectively, and allowed to stabilize for 24 h. The lower cell density for AlamarBlue® was used due to its higher sensitivity and prior optimization. Four experimental groups, each with triplicates, were assigned: Controls (negative and positive), DON-treated, ZEA-treated, and DON + ZEA combination-treated groups. Cells were exposed to treatments for 24, 48, and 72 h.

For the MTT assay, after exposure, the culture medium was removed, and 20 μL of 3-[4,5-dimethylthiazole-2-yl]-2,5-diphenyltetrazolium bromide (MTT; Sigma-Aldrich, Cat No. M5655) at 5 mg/mL in PBS was added to the wells along with 200 μL of 5 % FBS culture medium (Mosmann, 1983). The cells were then incubated at 37 °C in the dark for 2 h. Following incubation, the supernatant was discarded, 100 μL DMSO was added to solubilize the formazan crystals, and plates were agitated for 5 min. Absorbance was measured at 570 nm with background subtraction at 630 nm using a Synergy HT BioTek™ microplate reader (BIO-TEK Instruments, Vermont, USA). The percentage cell viability was calculated as follows:

$$Cell\ viability\left(\%\right) = \left(\frac{Absorbance\ of\ cells\ treated\ with\ mycotoxins}{Absorbance\ of\ cells\ treated\ with\ negative\ control}\right) \times 100$$

For the AlamarBlue® assay, at the end of the exposure period, the exposure medium was replaced with 100 μL of 10 % (v/v) AlamarBlue® Cell Viability Assay Reagent (Cat No. 1025, Thermo Fisher Scientific) in 5 % FBS culture medium and incubated for 2 h at 37 °C (Ibrahim et al., 2023). Fluorescence was measured at excitation 530 ± 25 nm and emission 590 ± 35 nm using a Synergy HT BioTek™ multi-mode microplate reader with 35 % fluorescence gain settings. Cell viability was determined after subtracting the AlamarBlue® reduction in media blanks from both negative controls and treatments and expressed as a percentage of the negative control.

2.4. Evaluation of F-actin and β-tubulin organization

Cytoskeletal protein analysis was conducted following a previously described protocol (Ibrahim et al., 2023). Briefly, Leydig cells were seeded at a density of 2.5×10^4 cells/well in 24-well plates and incubated overnight in EMEM medium containing 5 % FBS. Cells were then treated for 48 h with 0.1 and 0.4 μM DON, 20 and 60 μM ZEA, and their combinations (0.05 + 10 μM and 0.2 + 30 μM). Cytochalasin D and vinblastine sulfate (Sigma-Aldrich) were used as positive controls for F-actin and β-tubulin, respectively. Following treatment, cells were gently washed with PBS and fixed in ice-cold 100 % acetone (Merck) at −20 °C for 10 min and washed twice with PBS. For F-actin labeling, cells were incubated with FITC-phalloidin (Sigma-Aldrich) at 1 μg/mL for 30 min at 37 °C. For β-tubulin staining, cells were first blocked with 1 % bovine serum albumin (BSA) in PBS for 10 min at 37 °C, then incubated with a mouse anti-β-tubulin-Cy3 antibody (Sigma-Aldrich) at a 1:100 dilution for 1 h at 37 °C. After three PBS washes, cells were counterstained with DAPI (1.3 μg/mL) for 15 min at 37 °C, followed by three PBS washes. Coverslips were mounted using Prolong Gold Antifade (Invitrogen). Images were acquired using a Zeiss LSM-880 confocal microscope equipped with a 63 × oil immersion objective. Image processing was performed using custom Python scripts and the czifile library (v2019.7.2) for multidimensional image handling (Christoph, 2019).

2.5. Mitochondrial morphology

Leydig cells were seeded in 24-well plates at 2.5×10^4 cells/well and incubated overnight in 5 % FBS culture medium prior to experimental treatment. Following overnight incubation, cells were exposed to 0.1 and 0.4 μM DON, 20 and 60 μM ZEA, or their combinations (0.05 + 10 and 0.2 + 30 μM) for 48 h under standard culture conditions. For mitochondrial morphology assessment, we followed the same protocol described by Ibrahim et al. (2023). Briefly, 0.4 μM MitoTracker® Orange CMTMRos staining (Thermo Fisher Scientific) was followed by DAPI nuclear counterstaining and fixation with 4 % formalin. Post-fixation, cells were treated with ice-cold acetone and mounted with Prolong Gold Antifade (Invitrogen). Images were captured using confocal microscopy (Zeiss LSM-880×, 63 × oil objective) with standardized Z-stack acquisition parameters and saved in Carl Zeiss Image (CZI) format for analysis.

To quantify mitochondrial morphology and network connectivity, a custom automated image analysis pipeline was developed using Python (Chu et al., 2022). Confocal Z-stack images in CZI format were imported using the czifile library (Gohlke, 2013) and converted to maximum intensity projections to enhance mitochondrial structure visualization. Image pre-processing was performed using the scikit-image library (Van der Walt et al., 2014), with additional support from NumPy (Harris et al., 2020), SciPy (Virtanen et al., 2020), and Matplotlib (Hunter, 2007) for numerical analysis and visualization. Pre-processing steps included Gaussian filtering ($\sigma = 1.0$) to reduce background noise, followed by automated binarization using Otsu's thresholding method (Otsu, 1975). Morphological refinements were then applied to the binary masks, including removal of small objects (≥10 pixels), binary closing using a disk structuring element (radius = 2 pixels), and hole filling to reconstruct fragmented mitochondrial networks (Soille, 1999). Individual mitochondria were segmented via connected component labeling. Morphometric features were extracted using regionprops and included area, perimeter, major and minor axis lengths, eccentricity, and solidity. From these measurements, additional parameters were computed: aspect ratio (AR), defined as the ratio of major to minor axis lengths, and the form factor (FF), calculated as $FF = (4\pi \times Area)/Perimeter^2$, serving as an indicator of mitochondrial elongation and branching. The area fraction, representing the total mitochondrial area proportion of the total image area, was also calculated. Mitochondrial network connectivity was assessed using morphological skeletonization algorithms (Zhang and Suen, 1984), which reduced mitochondrial structures to their central axes. The resulting skeletons enabled quantification of total network length and identification of branch points, defined as skeleton pixels with more than two neighbors within a 3 × 3 pixel kernel. A connectivity index was subsequently derived to evaluate the integrity and complexity of the mitochondrial network based on branching architecture and continuity.

2.6. Assessment of lysosomal acidification

Lysosomal pH changes in Leydig cells were assessed using LysoSensor™ Green DND-189 (Invitrogen™, Thermo Fisher Scientific) following established protocols. Cells were treated with DON (0.1 and 0.4 μM), ZEA (20 and 60 μM), or their binary combinations (0.05 + 10 and 0.2 + 30 μM) for 48 h. Following exposure, cells underwent two PBS washes before a 30 min incubation at 37 °C with 1 μM LysoSensor™ Green DND-189 dissolved in serum-free and antibiotic-free EMEM medium. Subsequently, cells were subjected to two PBS rinses with gentle agitation, then prepared for microscopy using Prolong Gold Antifade mounting medium (Invitrogen). Images were captured using confocal microscopy (Zeiss LSM-880×, 63 × oil objective) and intensity was analysed using scikit-image and scipy in Python (Van der Walt et al., 2014).

2.7. Electron microscopy

For transmission electron microscopy (TEM), Leydig cells were seeded in 6-well plates at a density of 5×10^5 cells/well and allowed to attach overnight. Following 48 h exposure, cells were fixed in 2.5 % glutaraldehyde in 0.075 M phosphate buffer (pH 7.4) for 2 h at 4 °C. The fixed cells were scraped off, transferred to 2 ml Eppendorf tubes, and centrifuged at 1000×*g* for 3 min. Cell pellets were subsequently processed for TEM preparation following the same method described by Ibrahim et al. (2023) and Henn et al. (2024). Micrographs were acquired using a JEOL JEM 1400-FLASH transmission electron microscope (JEOL, Japan).

For scanning electron microscopy (SEM), Leydig cells were cultured on glass coverslips placed in 24-well plates at 2.5×10^4 cells/well for 24 h before being exposed. Following 48 h exposure to mycotoxins, coverslips were fixed with 2.5 % glutaraldehyde in 0.075 M phosphate buffer (pH 7.4) for 24 h at 4 °C, followed by post-fixation with 1 % osmium tetroxide for 2 h at room temperature. Samples were subsequently processed for SEM preparation according to Henn et al. (2024). Briefly, fixed samples were dehydrated, critical point dried, and sputter-coated with gold-palladium. Micrographs were acquired using a FEGSEM Zeiss Sigma 540 Ultra SEM (Carl Zeiss, Germany).

2.8. Statistical analysis

Cell viability percentages for MTT and AlamarBlue® assays were calculated using Microsoft Excel. Statistical analyses were conducted

using IBM SPSS Statistics version 28. A homogeneity of variances test was performed to assess normality, and the significant differences between concentrations were determined using one-way analysis of variance (ANOVA) followed by Tukey's HSD multiple range post hoc test. A p-value of ≤ 0.05 was considered significant. To determine the half-maximal inhibitory concentration (IC_{50}), a four-parameter logistic regression model was fitted to the dose-response data using Python v3.13.3 (Van Rossum and Python development team, 2025) implemented in Visual Studio Code v1.99.3 (Microsoft Corporation, 2023). The model was defined as:

$$y = Bottom + \frac{Top - Bottom}{1 + \left(\frac{x}{IC_{50}}\right)^{Hill}}$$

Where:

y = cell viability (%)

x = mycotoxin concentration (μM)

Bottom, *Top* = minimum and maximum responses

IC_{50} = concentration that reduces response by 50%

Hill = slope of the curve

Curve fitting was performed using the curve-fit function from the SciPy package (Virtanen et al., 2020), with parameter constraints to ensure biologically meaningful outputs. Initial values were estimated based on dataset characteristics to aid convergence (Motulsky and Christopoulos, 2004). Model performance was evaluated using the coefficient of determination (R^2), representing the proportion of variability explained by the model. All experiments were repeated at least three times. Descriptive statistics and curve visualization were performed using matplotlib (Hunter, 2007).

Furthermore, the interaction between deoxynivalenol (DON) and zearalenone (ZEA) was evaluated using the Bliss independence model (Bliss, 1939; Szabó et al., 2018) using Python v3.13.3 (Van Rossum and Python development team, 2025). This model assumes that two compounds act independently through different mechanisms and predicts the expected combined effect based on their individual cytotoxic effects. For DON and ZEA with individual effects E_{DON} and E_{ZEA}, the expected combined effect ($E_{DON\ +\ ZEA}$) is calculated as:

$$E_{DON+ZEA} = E_{DON} - E_{ZEA}\left(\frac{E_{DON} \times E_{ZEA}}{100}\right)$$

Where:

E_{DON} = effect of compound DON alone (100% − viability)

E_{ZEA} = effect of compound ZEA alone (100% − viability)

$E_{DON+ZEA}$ = expected combined effect

The expected combined viability is then calculated as:

$$Expected\ viability = 100 - E_{DON+ZEA}$$

The interactions were classified based on the deviation between observed and expected effects as synergistic (observed viability < expected viability), additive (observed viability ≈ expected viability) or antagonistic (observed viability > expected viability) (Chou, 2006; Foucquier and Guedj, 2015).

3. Results

3.1. Comparative cytotoxic effects of ZEA and DON

The cytotoxic effects of DON, ZEA, and their binary combinations were evaluated in LC-540 Leydig cells following 24, 48, and 72 h of exposure using MTT and AlamarBlue® metabolic activity assays (Fig. 1 and S1, S2).

Zearalenone exposure induced a time- and concentration-dependent decline in cell viability. The IC_{50} values determined from the MTT assay were 117.0, 69.1, and 34.4 μM at 24, 48, and 72 h, respectively. AlamarBlue® values revealed slightly greater sensitivity, with IC_{50} values of 97.6, 67.3, and 29.7 μM at the same respective time points. At the highest tested concentration (100 μM), ZEA induced a significant reduction in cell viability to 62.4 ± 1.4 %, 34.6 ± 3.0 %, and 27.2 ± 2.6 % using the MTT assay and 58.0 ± 2.2 %, 35.4 ± 0.5 %, and 20.0 ± 1.5 % with the AlamarBlue® assay at 24, 48, and 72 h, respectively (Fig. 1 and S1).

Comparatively, DON exhibited markedly higher cytotoxic potency. IC_{50} values from the MTT assay were 2.66, 0.50, and 0.44 μM at 24, 48, and 72 h, while corresponding values from the AlamarBlue® assay were 4.55, 0.60, and 0.40 μM. At 10 μM DON, MTT assay results indicated reductions in viability to 70.7 ± 2.8 %, 52.5 ± 8.5 %, and 38.2 ± 4.5 %, whereas AlamarBlue® revealed declines to 75.3 ± 2.4 %, 46.6 ± 0.6 %, and 27.7 ± 3.2 %, at 24, 48, and 72 h, respectively (Fig. 1 and S2).

3.2. Combined cytotoxic effects of ZEA and DON

Combined exposure to ZEA and DON resulted in concentration- and time-dependent interactions, as determined by the Bliss independence model (Fig. 1 and Table S1). At lower concentrations of 0.125 μM DON +10 μM ZEA, synergistic interactions were observed across all time points. Cell viability was reduced to 95.7 ± 7.9 %, 83.1 ± 4.8 %, and 71.0 ± 2.9 % by MTT assay, and to 98.7 ± 0.2 %, 79.9 ± 1.7 %, and 58.5 ± 3.1 % by AlamarBlue® assay after 24, 48, and 72 h, respectively. At concentrations of 2 μM DON +30 μM ZEA, the mycotoxin interaction transitioned from additive at 24 and 48 h to antagonistic at 72 h. Moreover, at concentrations of 5 μM DON +50 μM ZEA, an additive effect was observed after 24 h, but at 48 h and 72 h exposure, it was an antagonistic interaction.

3.3. Effects on F-actin and β-tubulin organization

Figs. 2 and 3 illustrate the fluorescence labeling of F-actin and β-tubulin in LC-540 Leydig cells following exposure to DON and ZEA, and their binary combinations for 48 h. In negative controls, polymerised F-actin microfilaments (green) exhibited a typical mesh-like structure, while β-tubulin filaments (red) formed a dense, organized microtubule network. Nuclei were counterstained with DAPI (blue). Positive controls included cytochalasin D, an inhibitor of actin polymerisation, and vinblastine sulfate, which disrupts microtubule formation. Treatment with cytochalasin D induced a marked disruption of F-actin filaments, whereas vinblastine sulfate caused a disorganized microtubule architecture, characterized by short, rod-like structures.

3.3.1. F-actin microfilament response

Following 48 h of exposure to 0.1 μM DON, the F-actin microfilament network remained fairly intact with slight disruption compared to either negative or positive controls. In contrast, 0.4 μM DON induced marked disruption and disorganization of the filament network with both peripheral aggregation and cytoplasmic condensation, displaying a granular appearance. Treatment with ZEA at 20 and 60 μM did not affect the structural integrity of F-actin filaments. However, combined exposure to 0.05 + 10 μM and 0.2 + 30 μM (DON + ZEA) caused peripheral and perinuclear filament aggregation, with more pronounced focal aggregation at the higher combined dose (red arrows in Fig. 2).

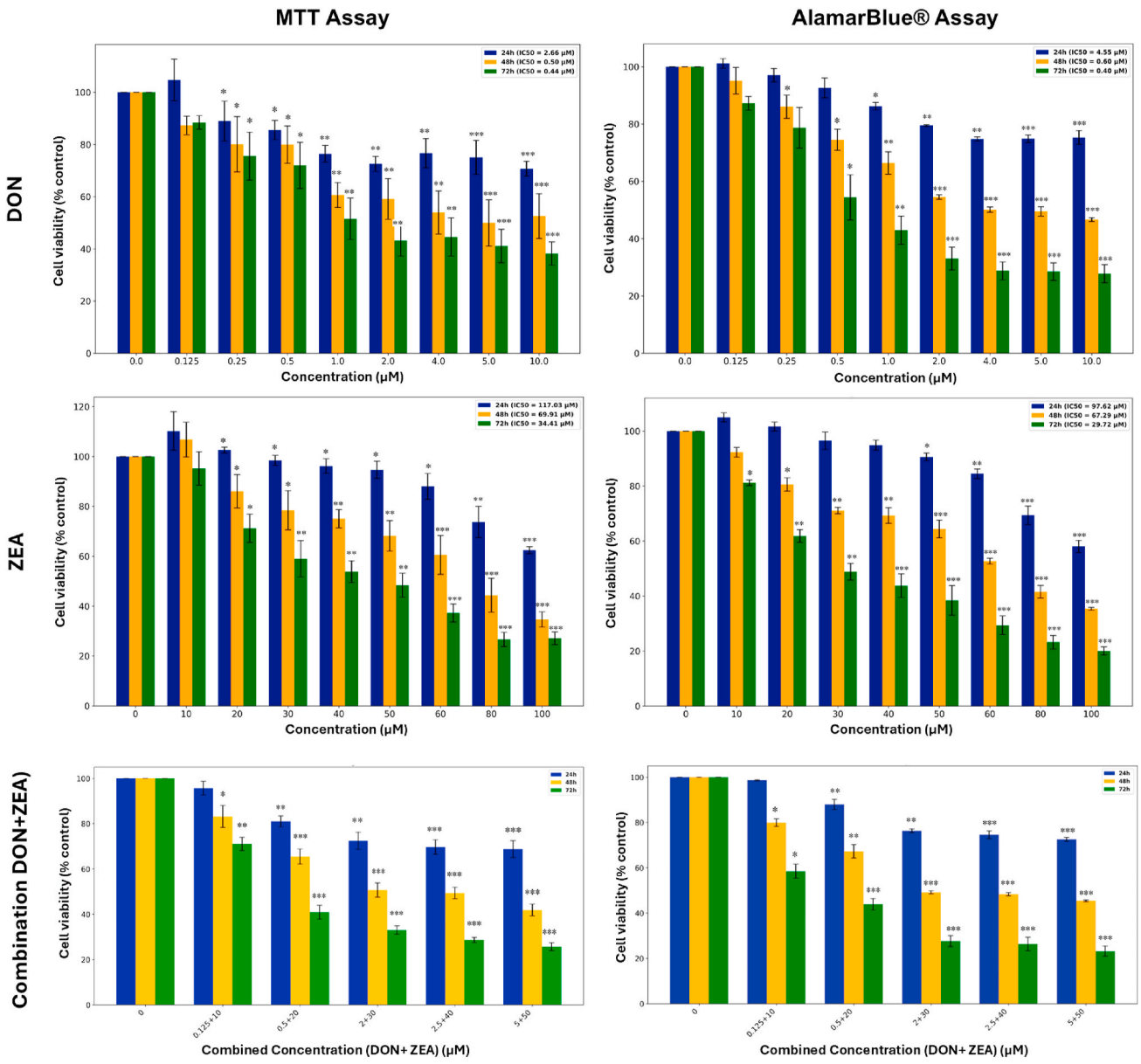

Fig. 1. Comparative cytotoxic effects of deoxynivalenol (DON) and zearalenone (ZEA) and their combination (DON + ZEA) on LC-540 Leydig cell viability. Cell viability was determined following exposure to ZEA, DON, and their combination for 24, 48 and 72h using MTT and AlamarBlue® assays. Results are expressed as a percentage of the untreated control and presented as the mean ± standard deviation (SD). Statistical significance is indicated as follows: ***$P < 0.001$, **$P < 0.01$, *$P < 0.05$.

3.3.2. *β-tubulin microtubule response*

After 48 h exposure to DON (0.1 and 0.4 μM), microtubules exhibited distinct perinuclear aggregation. Similarly, ZEA treatment disrupted microtubule architecture, with 20 μM inducing fragmentation and bundling, while 60 μM caused disorganization of microtubules accompanied by ring-like structures in the cytoplasm. In addition, combined exposure to DON and ZEA (0.05 + 10 μM and 0.2 + 30 μM) resulted in marked microtubule aggregation and disappearance (Fig. 3).

3.4. *Effects on mitochondrial morphology and lysosomal acidification*

Following 48 h of treatment with DON, ZEA, and their combination, Leydig cells were stained with the MitoTracker® Orange CMTMRos probe to assess mitochondrial morphology and network connectivity. Compared to the control group, treatment with ZEA at 60 μM and DON + ZEA at 0.2 + 30 μM for 48 h induced abnormal mitochondrial distribution in Leydig cell cytoplasm (Fig. 4A). Morphometric analyses evaluated mitochondrial size (area and perimeter), shape (form factor and aspect ratio), and network connectivity (number and length of mitochondrial branches) (Fig. 4B). Treatment with DON (0.1 and 0.4 μM) induced no significant alterations in mitochondrial morphological parameters compared to controls. However, exposure to ZEA at concentrations of 20 and 60 μM significantly decreased mitochondrial perimeter and branch number per mitochondrion, while the mean mitochondrial area was significantly reduced ($P < 0.01$) after exposure to 20 μM ZEA. In addition, combined treatment with DON + ZEA at 0.2 + 30 μM significantly reduced the mean area, mitochondrial perimeter, and branches per mitochondrion, suggesting increased mitochondrial damage under combined exposure conditions.

In addition, lysosomal acidity was assessed using LysoSensor™ Green DND-189 in Leydig cells after 48 h exposure to DON, ZEA, and their combinations (Fig. 4C). Treatments with DON (0.1 and 0.4 μM) or ZEA (20 and 60 μM) showed no significant increase in the lysosomal acidity ($p > 0.05$). However, combined DON + ZEA treatments (0.05 +

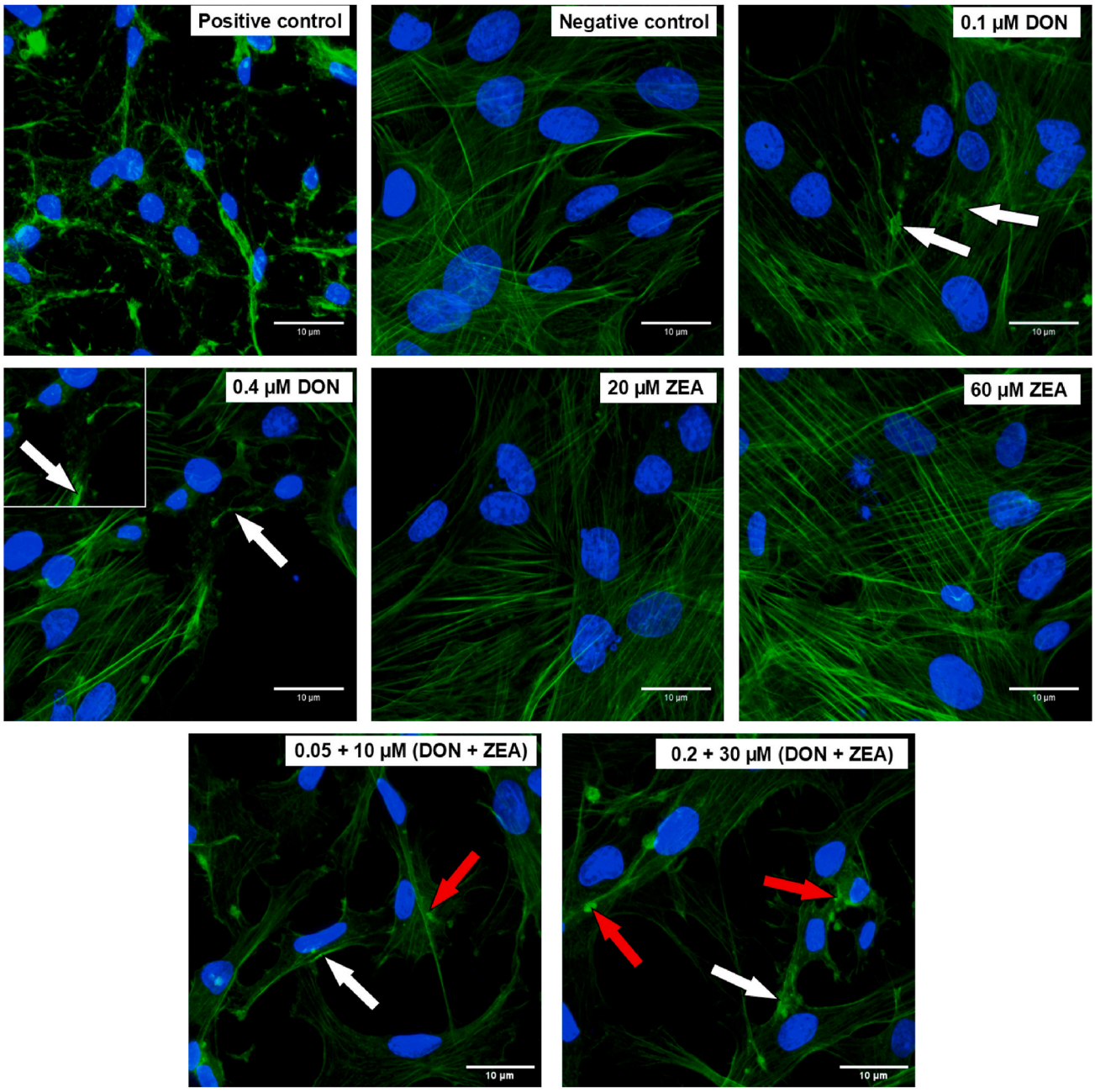

Fig. 2. Fluorescence labeling of F-actin microfilaments (green) in Leydig cells after 48 h exposure to DON and ZEA and their combination, stained with phalloidin-FITC. Cell nuclei were counterstained with DAPI (blue). Cytochalasin D was used as a positive control. White arrows indicate Leydig cells with peripheral filament network disorganization and localized disruption. Red arrows show perinuclear and focal aggregation of F-actin filaments. (For interpretation of the references to colour in this figure legend, the reader is referred to the Web version of this article.)

10 μM and 0.2 + 30 μM) significantly increased lysosomal acidification compared to controls (Fig. 4D), demonstrating that combined exposure triggers lysosomal acidification responses.

3.5. Ultrastructural alterations

The ultrastructural effects of 48 h exposure to DON and ZEA, individually and in combination, on Leydig cells were examined using transmission (TEM) and scanning (SEM) electron microscopy (Figs. 5 and 6). Control (untreated) cells exhibited normal morphology, characterized by intact mitochondria, a well-organized rough endoplasmic reticulum, and regular nuclear membranes, as well as a smooth cell surface with typical filopodial extensions (Fig. 5A–C). Exposure to DON at concentrations of 0.1 and 0.4 μM induced ultrastructural alterations. Changes included mitochondrial condensation, the formation of myelin figures composed of multiple concentric spherical rings, and the presence of lysosomes, autophagic vesicles and autolysosomes containing cytoplasmic organelles (Fig. 5D–I). However, SEM analysis revealed no obvious changes in cell surface following DON exposure. Treatment with 20 μM ZEA produced autophagosome formation, whereas exposure to 60 μM ZEA resulted in a marked loss of mitochondrial cristae, accompanied by membrane blebbing on the cell surface (Fig. 6A–C). Combined exposure to 0.05 + 10 μM DON + ZEA showed noticeable autolysosome containing a damaged organelle, while exposure to 0.2 μM DON and 30 μM ZEA caused severe ultrastructural damage, characterized by cytoplasmic vacuolation, mitochondrial damage, and apoptosis with chromatin condensation (Fig. 6G and H). These alterations were associated with characteristic features of apoptosis, including membrane blebbing

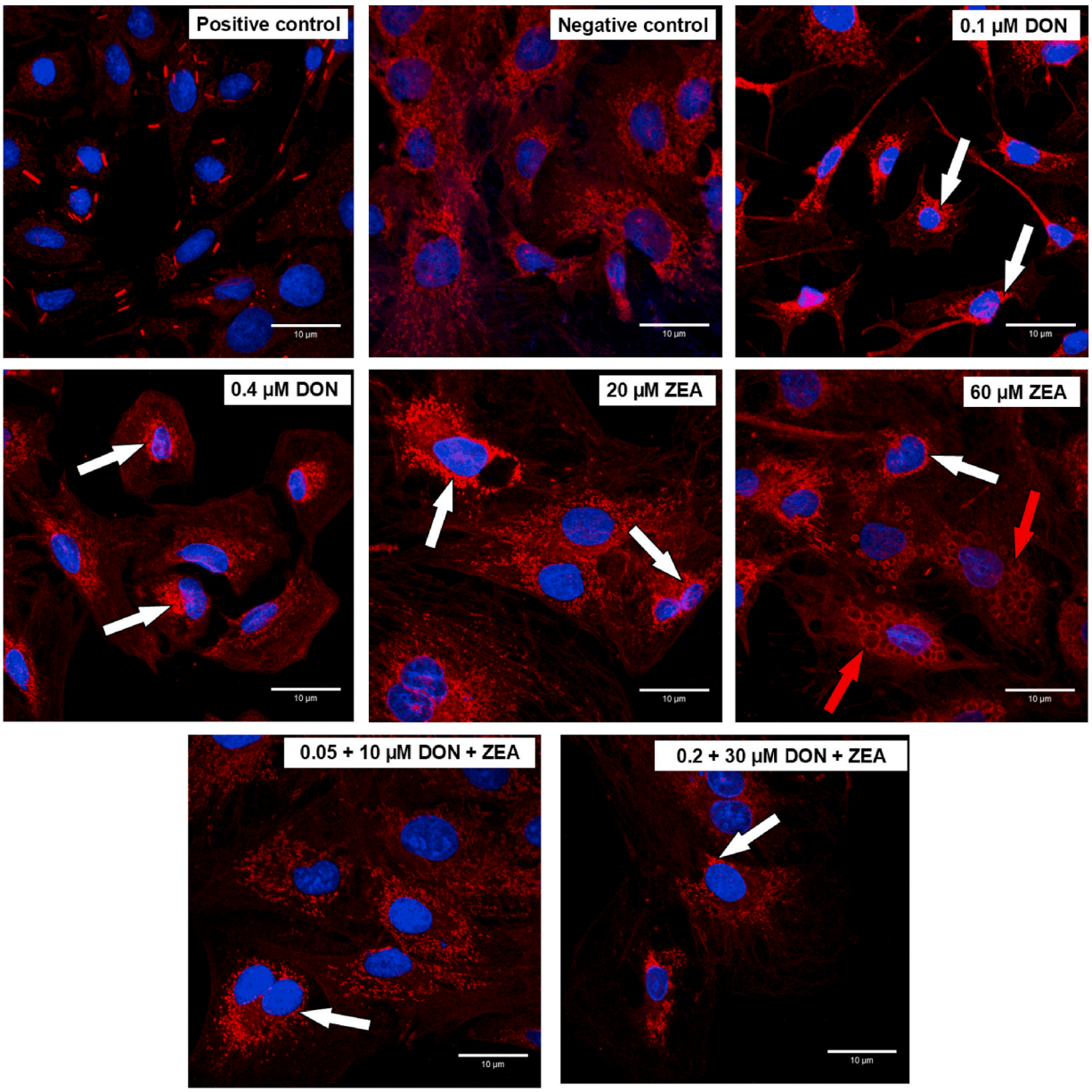

Fig. 3. Fluorescence labeling of microtubule network (red) in Leydig cells after 48 h exposure to DON and ZEA and their combination, stained with anti-β-tubulin-Cy3. Cell nuclei were counterstained with DAPI (blue). Vinblastine sulfate was used as a positive control. White arrows show disrupted microtubules and perinuclear aggregates. Red arrows indicate aggregation of microtubules forming ring-like structures in the cytoplasm of Leydig cells. (For interpretation of the references to colour in this figure legend, the reader is referred to the Web version of this article.)

and the formation of apoptotic bodies, clearly visible under SEM (Fig. 6I).

4. Discussion

The *Fusarium* mycotoxins, deoxynivalenol (DON) and zearalenone (ZEA), are well-known contaminants in cereal-based food and feed, with numerous adverse health effects. The male reproductive system is recognised as an important target organ (Tiemann and Dänicke, 2007). These mycotoxins have cytotoxic effects on Leydig cell lines (Eze et al., 2018; Savard et al., 2016; Sun et al., 2022). Savard et al. (2016) reported that DON at concentrations of 0.25 μM and 12.3 μM inhibited cell viability in MA-10 Leydig cells by 50 % after 24 h and 48 h exposure, respectively. In contrast, ZEA induced a 50 % effect at concentrations of 34 μM and 50.0 μM in the same cell line after 24 h (Savard et al., 2016), and 48 h (Eze et al., 2018) exposure, respectively. Moreover, at concentrations of 2.49 μM DON and 49.71 μM ZEA, a 50 % reduction in the viability were observed on isolated porcine Leydig cells (Sun et al., 2022). In our study, both DON and ZEA exhibited time- and concentration-dependent cytotoxicity in LC-540 Leydig cells. A 50 % cytotoxic effect induced by DON was observed at concentrations of (MTT: 2.66, 0.50, and 0.44 μM), and (AlamarBlue®: 4.55, 0.60, and 0.40 μm), after 24, 48 and 72 h, respectively. In comparison, the corresponding IC_{50} of ZEA was (MTT: 117.0, 69.1, and 34.4 μM) and (AlamarBlue®: 97.6, 67.3, and 29.7 μM), after 24, 48 and 72 h, respectively. The results indicated that Leydig cells are more sensitive to DON than ZEA, in which both assays delivered comparable IC_{50} values, with MTT measuring mitochondrial dehydrogenase activity and AlamarBlue® measuring metabolic activity.

Furthermore, ZEA has been reported to induce toxicity through various mechanisms that differ across cell types and dose levels (Zheng et al., 2018a). At low doses, ZEA exhibits estrogenic agonist activity by

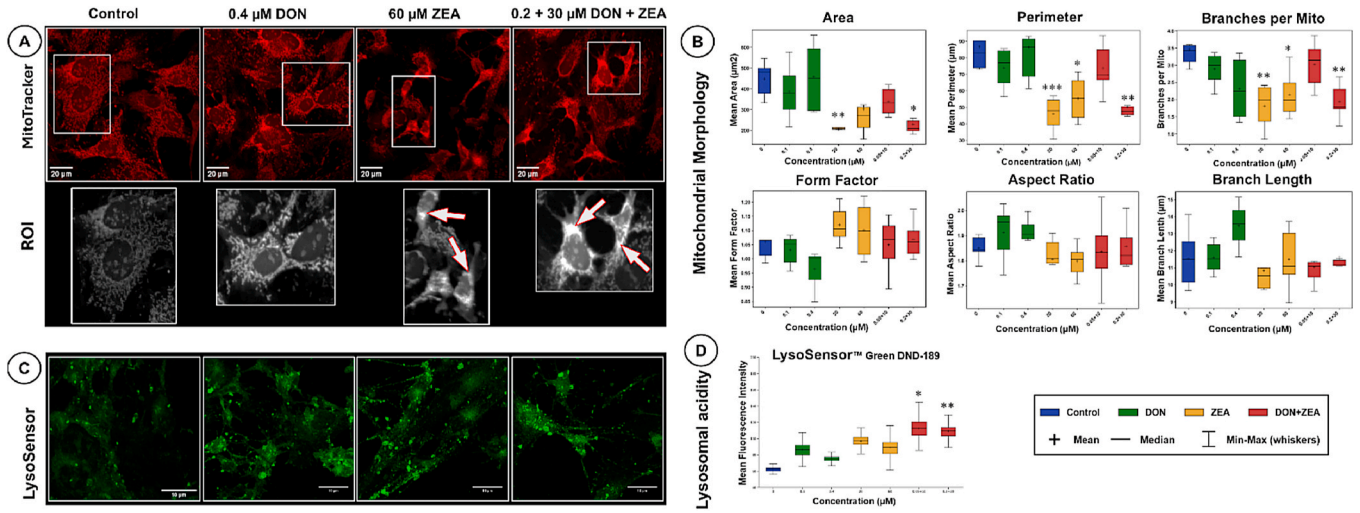

Fig. 4. Effect of 48 h exposure to deoxynivalenol (DON) and zearalenone (ZEA), alone and in combination, on mitochondrial morphology and lysosomal acidity in Leydig cells. (A) Mitochondria were stained with MitoTracker Orange (red). White boxes indicate regions of interest (ROI) shown at higher magnification in the lower panel. Scale bar = 20 μm. ROI: Higher magnification of the selected region displaying the distribution of mitochondria in the cytoplasm of Leydig cells. White arrows indicate fragmented mitochondria with abnormal cytoplasmic distribution in cells treated with 0.4 μM DON and 0.2 + 30 μM DON + ZEA combination. (B) Quantitative analysis of mitochondrial morphology (area and perimeter) and network connectivity (form factor, aspect ratio, branches/mito, and branch length) in control and treated groups (n = 3). (C) Lysosomal acidity was detected using LysoSensor™ Green DND-189 (green) in control and treated Leydig cells. Scale bar = 10 μm. (D) Quantification of mean fluorescence intensity of LysoSensor™ Green DND-189 showing lysosomal acidity levels across all treatment groups. All data are representative of three independent experiments and presented as box plots showing the interquartile range (IQR) with 1st quartile (Q1) and 3rd quartile (Q3). *, **, *** indicate statistical significance at $P \leq 0.05$, $P \leq 0.01$, and $P \leq 0.001$ compared to the control, respectively. (For interpretation of the references to colour in this figure legend, the reader is referred to the Web version of this article.)

promoting cell proliferation in Leydig cells (Wang et al., 2020; Zheng et al., 2017), while high-dose exposure induces cytotoxicity via apoptosis, immunotoxicity and DNA damage (Wang et al., 2020), mitochondrial damage and autophagy (Ben Salem et al., 2017). In the current study, we tested ZEA at higher concentrations (10 and 60 μM) to investigate mechanisms of cytotoxicity in male reproductive cells; however, caution must be applied when interpreting these cytotoxic findings to predict endocrine-disrupting effects, as humans are naturally exposed to lower concentrations in daily life.

Notably, combined exposure to ZEA and DON induced dose- and time-dependent cytotoxic interactions in LC-540 Leydig cells, according to the Bliss independence model. Combined exposure to 0.125 μM + 10 μM (DON + ZEA) induced synergistic cytotoxicity across all incubation periods. However, at concentrations of 2 μM + 30 μM and 5 μM + 50 μM (DON + ZEA) additive effects were observed at 24 and 48 h exposure, and antagonistic interactions at 72 h. Notably, other cell lines have also shown variable responses to DON and ZEA combined exposure, including synergistic effects in human hepatocytes (HepG2) and macrophages (RAW 264.7) (Xia et al., 2017; Zhou et al., 2017), as well as additive or antagonistic effects on human hepatocytes (BEL-7402) and monocytic leukemia cells (THP-1) (Gu et al., 2015; Smith et al., 2018). The variances in cellular responses to the effects of the combination of DON and ZEA have been attributed to exposure duration, concentration, and cell type-specific responses (Thapa et al., 2021). In this study, synergistic effects were observed at low concentrations, highlighting the potential reproductive risks caused by combined exposure to DON and ZEA at levels commonly detected in contaminated food and feed.

The current study also demonstrated that DON and ZEA can disrupt the structure of F-actin and β-tubulin in LC-540 Leydig cells. F-actin microfilaments and microtubules were depolymerized and disorganized after 48 h of treatment with DON, ZEA, and their combinations. The cytoskeletal proteins play a critical role in cholesterol trafficking from lipid droplets to mitochondria, which is an important step in testosterone biosynthesis (Hall and Almahbobi, 1992; Sewer and Li, 2008). Therefore, any structural alterations of these proteins affect steroidogenic processes. In previous *in vivo* and *in vitro* studies, it was concluded that DON and ZEA reduced testosterone production (Eze et al., 2018; Long et al., 2017; Song et al., 2022; Sprando et al., 2005). In the present study, we demonstrated that exposure to DON alone and in combination with ZEA depolymerized F-actin filaments and induced peripheral perinuclear aggregation in Leydig cells. Furthermore, cells exposed to DON and ZEA, or their combinations exhibited disorganization and abnormal ring-like structures of β-tubulin microtubules. To our knowledge, this is the first investigation to evaluate the effect of DON, ZEA and their combinations on cytoskeletal proteins in a Leydig cell model. Deoxynivalenol induces disruption of microtubules and microfilaments in mouse oocytes (Lan et al., 2018; Luo et al., 2025), while ZEA causes the disorganization of F-actin and α-tubulin in mouse Sertoli cells (TM4) (Zheng et al., 2018b). Both DON and ZEA have also been reported to downregulate key steroidogenic proteins and enzymes, such as steroidogenic acute regulatory protein (StAR) and 3β-hydroxysteroid dehydrogenase, and cholesterol side-chain cleavage in porcine and mouse Leydig cells (Song et al., 2022; Yang et al., 2007a). Therefore, this study suggests that disruption of cytoskeletal proteins in Leydig cells caused by DON, ZEA, or their combination may contribute to the decreased testosterone synthesis.

The present study also evaluated the effects of 48 h exposure to DON, ZEA, and their combination on mitochondrial morphology, lysosomal acidity, and ultrastructure in Leydig cells (Figs. 4–6). Zearalenone significantly altered mitochondrial area, perimeter, and branch number, and induced marked loss of cristae, as shown by TEM. Similar mitochondrial fragmentation and cristae rupture have been reported in porcine endometrial stromal cells (Hai et al., 2023) and piglet Sertoli cells (Ma et al., 2023) after 24 h of ZEA exposure. Recent evidence confirmed that ZEA disrupts mitochondrial dynamics through estrogen receptor 1-mediated pathways (Zhang et al., 2025). Leydig cells express estrogen receptors that play essential roles in regulating mitochondrial function (Yoh et al., 2023). In contrast to ZEA exposure, DON exposure produced different ultrastructural alterations, including myelin figures, autophagosomes (Fig. 5), autolysosomes, and increased lysosomal acidity, as revealed by LysoSensor Green DND-189 staining (Fig. 4). Deoxynivalenol-induced autophagy has been reported in various cell

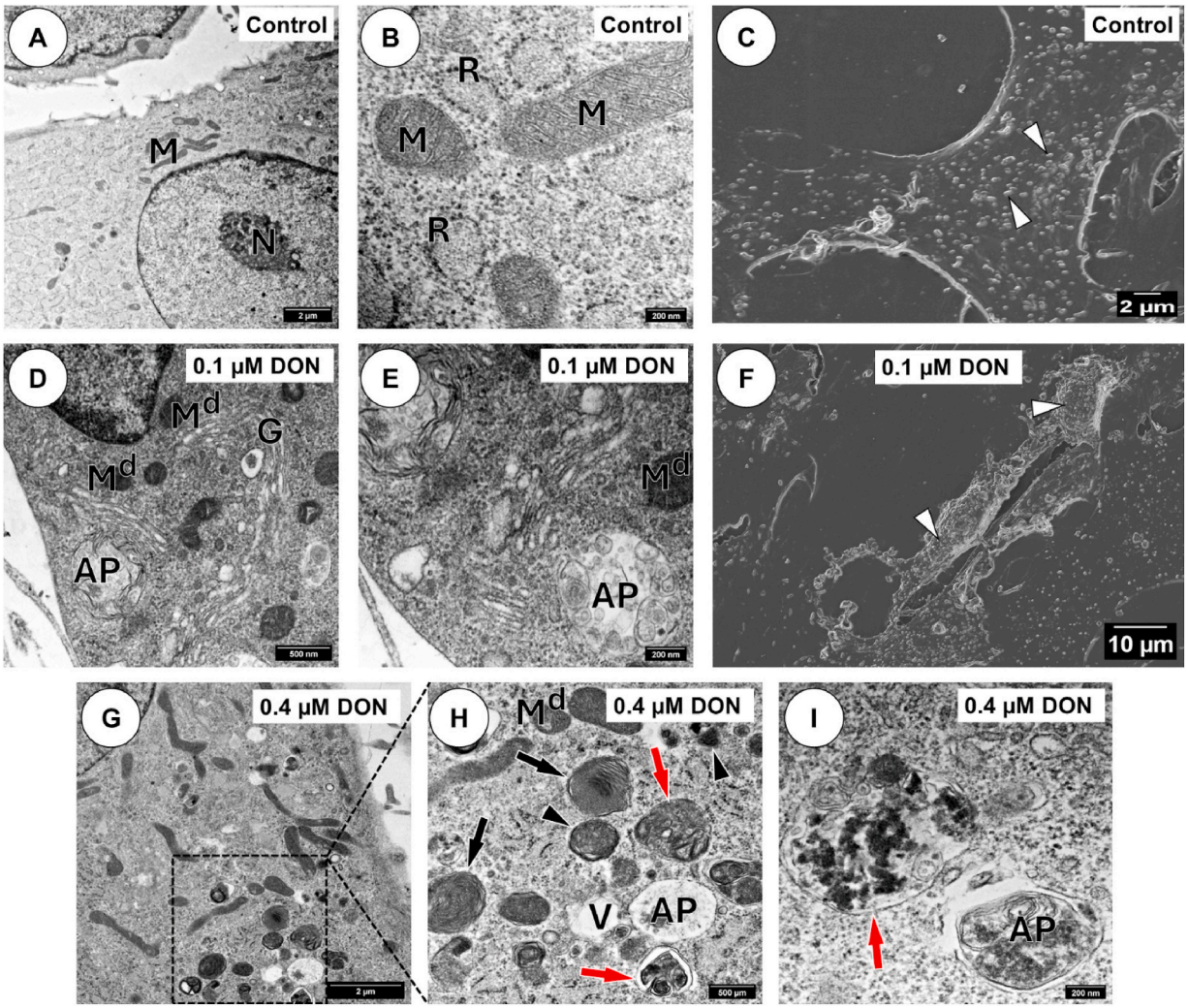

Fig. 5. Transmission and scanning electron micrographs of Leydig cells exposed to 0.1 and 0.4 µM deoxynivalenol (DON) for 48 h. White arrowheads indicate filopodial proliferation from the surface of cells. Black arrows: Myelin figures composed of multiple concentric spherical rings (damaged mitochondria). Black arrowheads: Lysosomes. Red arrows indicate an autolysosome enclosing a damaged organelle. M: Normal mitochondria. M^d Damaged mitochondria. AP: Autophagosome. G: Golgi complex. R: rough endoplasmic reticulum. (For interpretation of the references to colour in this figure legend, the reader is referred to the Web version of this article.)

types, including porcine oocytes (Han et al., 2016), intestinal epithelial cells (Tang et al., 2015), and prostate epithelial cells (Kowalska et al., 2022). This mycotoxin can induce direct or indirect damage to organelles (Hou et al., 2023), which triggers autophagy as a protective response. Therefore, the increase in the lysosomal acidification observed in this study may indicate cellular responses to DON toxicity. Although autophagosomes were observed using TEM, future studies investigating autophagic markers such as LC3, Beclin-1, and p62 (Huppelschoten et al., 2023; Sharawy et al., 2025; Zhu et al., 2025), would provide deeper mechanistic insight into mycotoxin-induced Leydig cell cytotoxicity.

Notably, combined exposure to DON and ZEA induced marked morphological alterations, including mitochondrial damage, autolysosome formation, and apoptotic features such as membrane blebbing, accompanied by increased lysosomal acidity. These findings suggest that the cytotoxic effects of DON and ZEA combined exposure involve multiple cell death pathways mediated by distinct mechanisms. In previous studies combined exposure to DON and ZEA induced oxidative stress-mediated apoptosis (Liang et al., 2015; Ren et al., 2016, 2017; Zhang et al., 2018), triggered pro-apoptotic signalling (Ren et al., 2017; Sun et al., 2014), and induced mitochondrial dysfunction (Bensassi et al., 2014; Zhang et al., 2018).

Savard et al. (2016) reported that combined exposure to DON and ZEA reduced progesterone secretion in MA-10 Leydig cells, even when cell viability was restored through antioxidant treatment. This finding suggests that steroidogenic impairment involves mechanisms beyond oxidative stress alone. Furthermore, Sun et al. (2022) reported that both DON and ZEA decreased testosterone and progesterone secretion in porcine Leydig cells by downregulating the expression of the steroidogenic acute regulatory protein (StAR) and 3β-hydroxysteroid dehydrogenase (3β-HSD) enzyme. On the other hand, the expression of cytochrome P450 aromatase (CYP19A1) and cholesterol side-chain cleavage enzyme (CYP11A1) was inhibited in porcine granulosa cells after exposure to DON and ZEA (Ranzenigo et al., 2008). It has been demonstrated that cytoskeletal proteins are essential for trafficking cholesterol from lipid droplets into mitochondria (Andric and Kostic, 2019; Hall and Almahbobi, 1992; Sewer and Li, 2008)., while normal mitochondrial structure is critical for CYP11A1 enzyme activity and steroidogenesis (Chien et al., 2017) Therefore, the cytoskeletal proteins disruption (F-actin and β-tubulin) and mitochondrial damage induced by DON, ZEA or their combinations observed in this study, may provide an additional plausible explanation for steroidogenic failure.

In conclusion, this study reports for the first time the disruptive effects of DON and ZEA, individually or in combination, on F-actin

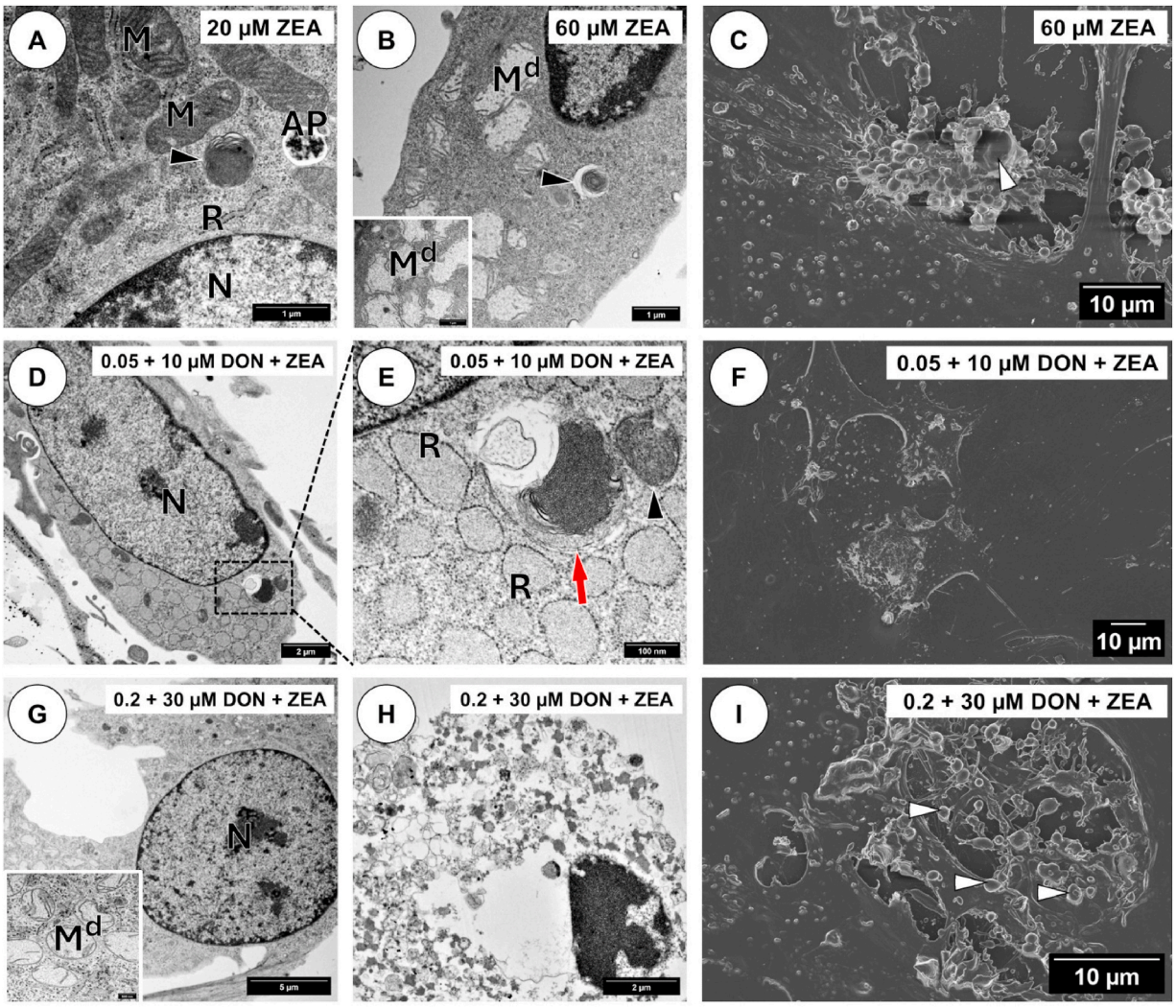

Fig. 6. Transmission and scanning electron micrographs of Leydig cells exposed to 20 and 60 μM zearalenone (ZEA) and combinations 0.05 + 10 μM and 0.2 + 30 μM deoxynivalenol and zearalenone (DON + ZEA) for 48 h. White arrowheads: Membrane blebbing in the surface of Leydig cells. Black arrowheads: Lysosomes. Red arrow indicates an autolysosome enclosing a damaged organelle. AP: Autophagosome. M: Normal mitochondria. M^d: Damaged mitochondria. G: Golgi complex. R: rough endoplasmic reticulum. (H) Late apoptotic Leydig cells with chromatin condensation and disrupted cellular membrane. (For interpretation of the references to colour in this figure legend, the reader is referred to the Web version of this article.)

microfilaments and microtubule cytoskeletal proteins in the LC-540 Leydig cell line. Individual exposure to DON and ZEA caused time- and concentration-dependent cytotoxicity. Combined exposure demonstrated synergistic effects at low concentrations (0.125 μM DON + 10 μM ZEA), while additive and antagonistic effects were observed at higher concentrations (5 μM DON + 50 μM ZEA) with increased exposure duration. This study also demonstrated that DON, ZEA, or their combination induce cytotoxicity in Leydig cells by disrupting the cytoskeleton and damaging mitochondria. These findings contribute to understanding the male reproductive toxicity induced by DON and ZEA.

CRediT authorship contribution statement

Mohammed I.A. Ibrahim: Writing – original draft, Investigation, Formal analysis, Conceptualization. **Antoinette V. Lensink:** Writing – review & editing, Visualization, Methodology. **Christo J. Botha:** Writing – review & editing, Project administration, Funding acquisition, Data curation, Conceptualization.

Declaration of competing interest

The authors declare that they have no known competing financial interests or personal relationships that could have appeared to influence the work reported in this paper.

Acknowledgments

The authors gratefully acknowledge Charity Maepa from the Microscopy and Microanalysis Unit at the University of Pretoria for her expert assistance with confocal and scanning electron microscopy. Mohammed Ibrahim acknowledges financial support from the University of Pretoria's Co-funded Postdoctoral Fellowship.

Appendix A. Supplementary data

Supplementary data to this article can be found online at https://doi.org/10.1016/j.fct.2025.115924.

Data availability

Data will be made available on request.

References

Adibnia, E., Razi, M., Malekinejad, H., 2016. Zearalenone and 17 β-estradiol induced damages in Male rats reproduction potential; evidence for ERα and ERβ receptors expression and steroidogenesis. Toxicon 120, 133–146. https://doi.org/10.1016/j.toxicon.2016.08.009.

Andric, S.A., Kostic, T.S., 2019. Regulation of Leydig cell steroidogenesis: intriguing network of signaling pathways and mitochondrial signalosome. Curr. Opin. Endocr. Metab. Res. 6, 7–20. https://doi.org/10.1016/j.coemr.2019.03.001.

Ben Salem, I., Boussabbeh, M., Da Silva, J.P., Guilbert, A., Bacha, H., Abid-Essefi, S., Lemaire, C., 2017. SIRT1 protects cardiac cells against apoptosis induced by zearalenone or its metabolites α- and β-zearalenol through an autophagy-dependent pathway. Toxicol. Appl. Pharmacol. 314, 82–90. https://doi.org/10.1016/j.taap.2016.11.012.

Bensassi, F., Gallerne, C., Sharaf el dein, O., Hajlaoui, M.R., Lemaire, C., Bacha, H., 2014. *In vitro* investigation of toxicological interactions between the fusariotoxins deoxynivalenol and zearalenone. Toxicon 84, 1–6. https://doi.org/10.1016/j.toxicon.2014.03.005.

Bliss, C.I., 1939. The toxicity of poisons applied jointly 1. Ann. Appl. Biol. 26, 585–615. https://doi.org/10.1111/j.1744-7348.1939.tb06990.x.

Cao, L., Zhao, J., Chen, L.-x., Xie, X., Ran, M., Shen, M.-y., Zhu, L., Feng, S.-b., Li, Y., Wu, J.-j., 2020a. Effects of combined exposure of zearalenone and deoxynivalenol on reproductive toxicity of male mice and alleviation of tea polyphenols. Chin. J. Anim. Nutr. 32, 1946–1956. https://doi.org/10.3969/j.issn.1006?267x.2020.04.055.

Cao, Z., Huang, W., Sun, Y., Li, Y., 2020b. Deoxynivalenol induced spermatogenesis disorder by blood-testis barrier disruption associated with testosterone deficiency and inflammation in mice. Environ. Pollut. 264, 114748. https://doi.org/10.1016/j.envpol.2020.114748.

Chien, Y., Rosal, K., Chung, B.-c., 2017. Function of CYP11A1 in the mitochondria. Mol. Cell. Endocrinol. 441, 55–61. https://doi.org/10.1016/j.mce.2016.10.030.

Chou, T.-C., 2006. Theoretical basis, experimental design, and computerized simulation of synergism and antagonism in drug combination studies. Pharmacol. Rev. 58, 621–681. https://doi.org/10.1124/pr.58.3.10.

Christoph, G., 2019. Czifile: read Carl Zeiss Image (CZI) files. Python Package Index. https://pypi.org/project/czifile/.

Chu, C.-H., Tseng, W.-W., Hsu, C.-M., Wei, A.-C., 2022. Image analysis of the mitochondrial network morphology with applications in cancer research. Front. Phys. 10–2022. https://doi.org/10.3389/fphy.2022.855775.

Clark, M.A., Shay, J.W., 1981. The role of tubulin in the steroidogenic response of murine adrenal and rat Leydig cells. Endocrinology 109, 2261–2263. https://doi.org/10.1210/endo-109-6-2261.

El-Sayed, R.A., Jebur, A.B., Kang, W., El-Demerdash, F.M., 2022. An overview on the major mycotoxins in food products: characteristics, toxicity, and analysis. J. Future Foods 2, 91–102. https://doi.org/10.1016/j.jfutfo.2022.03.002.

Eskola, M., Kos, G., Elliott, C.T., Hajšlová, J., Mayar, S., Krska, R., 2020. Worldwide contamination of food-crops with mycotoxins: validity of the widely cited 'FAO estimate' of 25%. Crit. Rev. Food Sci. Nutr. 60, 2773–2789. https://doi.org/10.1080/10408398.2019.1658570.

Eze, U.A., Huntriss, J., Routledge, M.N., Gong, Y.Y., 2018. Toxicological effects of regulated mycotoxins and persistent organochloride pesticides: in vitro cytotoxic assessment of single and defined mixtures on MA-10 murine Leydig cell line. Toxicol. Vitro 48, 93–103. https://doi.org/10.1016/j.tiv.2017.12.019.

Foucquier, J., Guedj, M., 2015. Analysis of Drug Combinations: current methodological landscape. Pharmacol. res. perspect. 3, e00149. https://doi.org/10.1002/prp2.149.

Ghedira-Chekir, L., Maaroufi, K., Creppy, E., Bacha, H., 1999. Cytotoxic and genotoxic effects of zearalenone: prevention by vitamin E. Toxicol. Toxin Rev 18, 355–368. https://doi.org/10.3109/15569549909009263.

Gohlke, C., 2013. Czifile: read Carl Zeiss image (CZI) files. Python package. https://www.lfd.uci.edu/~gohlke/code/czifile.py.html.

Gu, W., Zhu, P., Jiang, D., He, X., Li, Y., Ji, J., Zhang, L., Sun, Y., Sun, X., 2015. A novel and simple cell-based electrochemical impedance biosensor for evaluating the combined toxicity of DON and ZEN. Biosens. Bioelectron. 70, 447–454. https://doi.org/10.1016/j.bios.2015.03.074.

Hai, S., Zhao, J., Chen, C., Wang, C., Ma, L., Rahman, S.U., Zhao, C., Feng, S., Wu, J., Wang, X., 2023. Zearalenone promotes porcine ESCs apoptosis by enhancing Drp1-mediated mitochondrial fragmentation and activating the JNK pathway. Food Chem. Toxicol. 182, 114110. https://doi.org/10.1016/j.fct.2023.114110.

Hall, P.F., Almahbobi, G., 1992. The role of the cytoskeleton in the regulation of steroidogenesis. J. Steroid Biochem. Mol. Biol. 43, 769–777. https://doi.org/10.1016/0960-0760(92)90306-4.

Hallaj Salahipour, M., Hasanzadeh, S., Malekinejad, H., Razi, M., Farrokhi-Ardebili, F., 2019. Deoxynivalenol reduces quality parameters and increases DNA damage in mice spermatozoa. Andrologia 51, e13238. https://doi.org/10.1111/and.13238.

Han, J., Wang, Q.-C., Zhu, C.-C., Liu, J., Zhang, Y., Cui, X.-S., Kim, N.-H., Sun, S.-C., 2016. Deoxynivalenol exposure induces autophagy/apoptosis and epigenetic modification changes during porcine oocyte maturation. Toxicol. Appl. Pharmacol. 300, 70–76. https://doi.org/10.1016/j.taap.2016.03.006.

Harris, C.R., Millman, K.J., Van Der Walt, S.J., Gommers, R., Virtanen, P., Cournapeau, D., Wieser, E., Taylor, J., Berg, S., Smith, N.J., 2020. Array programming with NumPy. Nature 585, 357–362. https://doi.org/10.1038/s41586-020-2649-2.

Henn, D., Lensink, A.V., Botha, C.J., 2024. Ultrastructural changes in cardiac and skeletal myoblasts following in vitro exposure to monensin, salinomycin, and lasalocid. PLoS One 19, e0311046. https://doi.org/10.1371/journal.pone.0311046.

Hou, S., Ma, J., Cheng, Y., Wang, H., Sun, J., Yan, Y., 2023. The toxicity mechanisms of DON to humans and animals and potential biological treatment strategies. Crit. Rev. Food Sci. Nutr. 63, 790–812. https://doi.org/10.1080/10408398.2021.1954598.

Hueza, I.M., Raspantini, P.C.F., Raspantini, L.E.R., Latorre, A.O., Górniak, S.L., 2014. Zearalenone, an estrogenic mycotoxin, is an immunotoxic compound. Toxins 6, 1080–1095. https://doi.org/10.3390/toxins6031080.

Hunter, J.D., 2007. Matplotlib: a 2D graphics environment. Comput. Sci. Eng. 9, 90–95.

Huppelschoten, Y., Buchardt, J., Nielsen, T.E., Sapmaz, A., van der Heden van Noort, G. J., 2023. Total chemical synthesis of LC3A and LC3B activity-based probes. Biomedicines 11, 884. https://doi.org/10.3390/biomedicines11030884.

Ibrahim, M.I.A., Ferreira, G.C.H., Venter, E.A., Botha, C.J., 2023. Cytotoxicity, morphological and ultrastructural effects induced by the neonicotinoid pesticide, imidacloprid, using a rat Leydig cell line (LC-540). Environ. Toxicol. Pharmacol. 104, 104310. https://doi.org/10.1016/j.etap.2023.104310.

Kowalska, K., Kozieł, M.J., Habrowska-Górczyńska, D.E., Urbanek, K.A., Domińska, K., Piastowska-Ciesielska, A.W., 2022. Deoxynivalenol induces apoptosis and autophagy in human prostate epithelial cells via PI3K/Akt signaling pathway. Arch. Toxicol. 96, 231–241. https://doi.org/10.1007/s00204-021-03176-z.

Lan, M., Han, J., Pan, M.H., Wan, X., Pan, Z.N., Sun, S.C., 2018. Melatonin protects against defects induced by deoxynivalenol during mouse oocyte maturation. J. Pineal Res. 65, e12477. https://doi.org/10.1111/jpi.12477.

Lazzaretti, C., Roy, N., Paradiso, E., Capponi, C., Ferrari, T., Reggianini, F., Sperduti, S., Perri, C., Baschieri, L., Mascolo, E., Varani, M., Canu, G., Trenti, T., Nicoli, A., Morini, D., Iannotti, F., Villani, M.T., Vicini, E., Simoni, M., Casarini, L., 2024. Benzo [a]pyrene disrupts LH/hCG-dependent mouse Leydig cell steroidogenesis through receptor/Gαs protein targeting. Sci. Rep. 14, 844. https://doi.org/10.1038/s41598-024-51516-7.

Li, L., Zhang, T., Ren, X., Li, B., Wang, S., 2021. Male reproductive toxicity of zearalenone—Meta-analysis with mechanism review. Ecotoxicol. Environ. Saf. 221, 112457. https://doi.org/10.1016/j.ecoenv.2021.112457.

Li, Y., Wu, Q., Li, X., Cournoyer, P., Choudhuri, S., Guo, L., Chen, S., 2024. Toxicity of cannabidiol and its metabolites in TM3 mouse Leydig cells: a comparison with primary human Leydig cells. Arch. Toxicol. 98, 2677–2693. https://doi.org/10.1007/s00204-024-03754-x.

Liang, Z., Ren, Z., Gao, S., Chen, Y., Yang, Y., Yang, D., Deng, J., Zuo, Z., Wang, Y., Shen, L., 2015. Individual and combined effects of deoxynivalenol and zearalenone on mouse kidney. Environ. Toxicol. Pharmacol. 40, 686–691. https://doi.org/10.1016/j.etap.2015.08.029.

Long, M., Yang, S., Dong, S., Chen, X., Zhang, Y., He, J., 2017. Characterization of semen quality, testicular marker enzyme activities and gene expression changes in the blood testis barrier of Kunming mice following acute exposure to zearalenone. Environ. Sci. Pollut. Res. Int. 24, 27235–27243. https://doi.org/10.1007/s11356-017-0299-1.

Luo, H., Chen, J., Guo, Z., Zhu, Y., Wang, Y., Wu, T., Yin, S., Li, C., Su, Y., Chen, Y., Qian, Y., Miao, C., Feng, R., 2025. Tubacin alleviate the reproductive toxicity of deoxynivalenol in mouse oocytes and zygotes via strengthening microtubule stability. Cell Commun. Signal. 23, 417. https://doi.org/10.1186/s12964-025-02432-4.

Ma, L., Hai, S., Wang, C., Chen, C., Rahman, S.U., Zhao, C., Bazai, M.A., Feng, S., Wang, X., 2023. Zearalenone induces mitochondria-associated endoplasmic reticulum membranes dysfunction in piglet Sertoli cells based on endoplasmic reticulum stress. Ecotoxicol. Environ. Saf. 254, 114710. https://doi.org/10.1016/j.ecoenv.2023.114710.

Microsoft Corporation, 2023. Visual Studio Code. Computer software, Version 1.99.3. https://code.visualstudio.com/.

Mosmann, T., 1983. Rapid colorimetric assay for cellular growth and survival: application to proliferation and cytotoxicity assays. J. Immunol. Methods 65, 55–63.

Motulsky, H., Christopoulos, A., 2004. Fitting Models to Biological Data Using Linear and Nonlinear Regression: a Practical Guide to Curve Fitting. Oxford University Press.

Otsu, N., 1975. A threshold selection method from gray-level histograms. Automatica 11, 23–27.

Papadopoulos, V., Miller, W.L., 2012. Role of mitochondria in steroidogenesis. Best Pract. Res. Clin. Endocrinol. Metabol. 26, 771–790. https://doi.org/10.1016/j.beem.2012.05.002.

Pestka, J.J., 2010. Deoxynivalenol: mechanisms of action, human exposure, and toxicological relevance. Arch. Toxicol. 84, 663–679. https://doi.org/10.1007/s00204-010-0579-8.

Ranzenigo, G., Caloni, F., Cremonesi, F., Aad, P.Y., Spicer, L.J., 2008. Effects of Fusarium mycotoxins on steroid production by porcine granulosa cells. Anim. Reprod. Sci. 107, 115–130. https://doi.org/10.1016/j.anireprosci.2007.06.023.

Ren, Z., Deng, H., Deng, Y., Liang, Z., Deng, J., Zuo, Z., Hu, Y., Shen, L., Yu, S., Cao, S., 2017. Combined effects of deoxynivalenol and zearalenone on oxidative injury and apoptosis in porcine splenic lymphocytes in vitro. Exp. Toxicol. Pathol. 69, 612–617. https://doi.org/10.1016/j.etp.2017.05.008.

Ren, Z.H., Deng, H.D., Deng, Y.T., Deng, J.L., Zuo, Z.C., Yu, S.M., Shen, L.H., Cui, H.M., Xu, Z.W., Hu, Y.C., 2016. Effect of the Fusarium toxins, zearalenone and deoxynivalenol, on the mouse brain. Environ. Toxicol. Pharmacol. 46, 62–70. https://doi.org/10.1016/j.etap.2016.06.028.

Savard, C., Nogues, P., Boyer, A., Chorfi, Y., 2016. Prevention of deoxynivalenol- and zearalenone-associated oxidative stress does not restore MA-10 Leydig cell functions. Toxicology 341–343, 17–27. https://doi.org/10.1016/j.tox.2016.01.003.

Serviento, A.M., Brossard, L., Renaudeau, D., 2018. An acute challenge with a deoxynivalenol-contaminated diet has short- and long-term effects on performance and feeding behavior in finishing pigs. J. Anim. Sci. 96, 5209–5221. https://doi.org/10.1093/jas/sky378.

Sewer, M.B., Li, D., 2008. Regulation of steroid hormone biosynthesis by the cytoskeleton. Lipids 43, 1109–1115. https://doi.org/10.1007/s11745-008-3221-2.

Sharawy, M.H., Abdel-Rahman, A.M., Abdel-Rahman, N., 2025. Aprepitant ameliorates vancomycin-induced kidney injury: role of GPX4/system Xc− and oxidative damage. Food Chem. Toxicol. 197, 115264. https://doi.org/10.1016/j.fct.2025.115264.

Smith, M.-C., Madec, S., Troadec, S., Coton, E., Hymery, N., 2018. Effects of fusariotoxin co-exposure on THP-1 human immune cells. Cell Biol. Toxicol. 34, 191–205. https://doi.org/10.1007/s10565-017-9408-7.

Sobrova, P., Adam, V., Vasatkova, A., Beklova, M., Zeman, L., Kizek, R., 2010. Deoxynivalenol and its toxicity. Interdiscip. Toxicol. 3, 94–99. https://doi.org/10.2478/v10102-010-0019-x.

Soille, P., 1999. Morphological Image Analysis: Principles and Applications. Springer.

Song, J.-L., Sun, Y.-J., Liu, G.-Q., Zhang, G.-L., 2022. Deoxynivalenol and zearalenone: different mycotoxins with different toxic effects in donkey (Equus asinus) endometrial epithelial cells. Theriogenology 179, 162–176. https://doi.org/10.1016/j.theriogenology.2021.11.021.

Sprando, R.L., Collins, T.F.X., Black, T.N., Olejnik, N., Rorie, J.I., Eppley, R.M., Ruggles, D.I., 2005. Characterization of the effect of deoxynivalenol on selected male reproductive endpoints. Food Chem. Toxicol. 43, 623–635. https://doi.org/10.1016/j.fct.2004.12.017.

Sun, L.-H., Lei, M.-y., Zhang, N.-Y., Zhao, L., Krumm, C.S., Qi, D.-S., 2014. Hepatotoxic effects of mycotoxin combinations in mice. Food Chem. Toxicol. 74, 289–293. https://doi.org/10.1016/j.fct.2014.10.020.

Sun, L., Dai, J., Xu, J., Yang, J., Zhang, D., 2022. Comparative cytotoxic effects and possible mechanisms of deoxynivalenol, Zearalenone and T-2 toxin exposure to porcine Leydig cells in vitro. Toxins 14, 113. https://doi.org/10.3390/toxins14020113.

Szabó, A., Szabó-Fodor, J., Fébel, H., Mézes, M., Balogh, K., Bázár, G., Kocsó, D., Ali, O., Kovács, M., 2018. Individual and combined effects of Fumonisin B1, deoxynivalenol and Zearalenone on the hepatic and renal membrane lipid integrity of rats. Toxins 10, 4. https://doi.org/10.3390/toxins10010004.

Takemura, H., Shim, J.Y., Sayama, K., Tsubura, A., Zhu, B.T., Shimoi, K., 2007. Characterization of the estrogenic activities of zearalenone and zeranol in vivo and in vitro. J. Steroid Biochem. Mol. Biol. 103, 170–177. https://doi.org/10.1016/j.jsbmb.2006.08.008.

Tang, Y., Li, J., Li, F., Hu, C.-A.A., Liao, P., Tan, K., Tan, B., Xiong, X., Liu, G., Li, T., Yin, Y., 2015. Autophagy protects intestinal epithelial Cells against Deoxynivalenol toxicity by alleviating oxidative stress via IKK signaling pathway. Free Radic. Biol. Med. 89, 944–951. https://doi.org/10.1016/j.freeradbiomed.2015.09.012.

Thapa, A., Horgan, K.A., White, B., Walls, D., 2021. Deoxynivalenol and zearalenone-synergistic or antagonistic agri-food chain Co-Contaminants? Toxins 13. https://doi.org/10.3390/toxins13080561.

Tiemann, U., Dänicke, S., 2007. In vivo and in vitro effects of the mycotoxins zearalenone and deoxynivalenol on different non-reproductive and reproductive organs in female pigs: a review. Food Addit. Contam. 24, 306–314. https://doi.org/10.1080/02652030601053626.

Van der Walt, S., Schönberger, J.L., Nunez-Iglesias, J., Boulogne, F., Warner, J.D., Yager, N., Gouillart, E., Yu, T., 2014. scikit-image: image processing in Python. PeerJ 2, e453. https://doi.org/10.7717/peerj.453.

Van Rossum, G., 2025. Python development team. Python. Python Software Foundation [Programming language], Version 3.13.3. https://www.python.org/.

Virtanen, P., Gommers, R., Oliphant, T., Haberland, M., Reddy, T., Cournapeau, D., Burovski, E., Peterson, P., Weckesser, W., Bright, J., 2020. Fundamental algorithms for scientific computing in python and SciPy 1.0 contributors. SciPy 1.0. Nat. Methods 17, 261–272. https://doi.org/10.1038/s41592-019-0686-2.

Wang, M., Yang, S., Cai, J., Yan, R., Meng, L., Long, M., Zhang, Y., 2020. Proteomic analysis using iTRAQ technology reveals the toxic effects of zearalenone on the leydig cells of rats. Food Chem. Toxicol. 141, 111405. https://doi.org/10.1016/j.fct.2020.111405.

Widodo, O.S., Uno, S., Kokushi, E., Yamato, O., Mardianto, M.F.F., Shinya, U., Kano, Y., Kawashima, C., Fushimi, Y., Ono, T., Taniguchi, M., Takagi, M., 2024. Exposure of cattle breeding herds to naturally Co-Contaminated zearalenone and deoxynivalenol: the relevance of a urinary mycotoxin monitoring system for herd health and food safety. Toxins 16. https://doi.org/10.3390/toxins16090402.

World Health Organization & Food and Agriculture Organization of the United Nations, 2011. World Health Organization & Food and Agriculture Organization of the United Nations (2011)Application of Risk Analysis Principles and Procedures During Food Safety Emergencies. Food and Agriculture Organization of the United Nations, Rome.

Wu, Z., Zhang, C., 2022. Role of the Cytoskeleton in steroidogenesis. Endocr., Metab. Immune Disord.: Drug Targets 22, 549–557. https://doi.org/10.2174/1871530321666211119143653.

Xia, S., Zhu, P., Pi, F., Zhang, Y., Li, Y., Wang, J., Sun, X., 2017. Development of a simple and convenient cell-based electrochemical biosensor for evaluating the individual and combined toxicity of DON, ZEN, and AFB1. Biosens. Bioelectron. 97, 345–351. https://doi.org/10.1016/j.bios.2017.06.002.

Yadav, S., Singh, V.P., 2021. Alternatives to animal experiments in research and regulatory testing. In: Nagarajan, P., Gudde, R., Srinivasan, R. (Eds.), Essentials of Laboratory Animal Science: Principles and Practices. Springer Singapore, Singapore, pp. 137–156. https://doi.org/10.1007/978-981-16-0987-9_7.

Yang, J.-h., Wang, J.-h., Guo, W.-b., Ling, A.-r., Luo, A.-q., Liu, D., Yang, X.-l., Zhao, Z.-h., 2019. Toxic effects and possible mechanisms of deoxynivalenol exposure on sperm and testicular damage in BALB/c mice. J. Agric. Food Chem. 67, 2289–2295. https://doi.org/10.1021/acs.jafc.8b04783.

Yang, J., Ye, L., Cui, R., Zheng, K., Qiao, X., Wang, M., Su, M., Li, X., Ge, R.S., Wang, Y., 2024. Deoxynivalenol Inhibits Progenitor Leydig cell development by stimulating mitochondrial fission in rats. J. Agric. Food Chem. 72, 10616–10626. https://doi.org/10.1021/acs.jafc.4c01151.

Yang, J., Zhang, Y., Wang, Y., Cui, S., 2007a. Toxic effects of zearalenone and α-zearalenol on the regulation of steroidogenesis and testosterone production in mouse Leydig cells. Toxicol. Vitro 21, 558–565. https://doi.org/10.1016/j.tiv.2006.10.013.

Yang, J.Y., Wang, G.X., Liu, J.L., Fan, J.J., Cui, S., 2007b. Toxic effects of zearalenone and its derivatives α-zearalenol on male reproductive system in mice. Reprod. Toxicol. 24, 381–387. https://doi.org/10.1016/j.reprotox.2007.05.009.

Yoh, K., Ikeda, K., Horie, K., Inoue, S., 2023. Roles of Estrogen, Estrogen receptors, and Estrogen-Related receptors in skeletal muscle: regulation of mitochondrial function. Int. J. Mol. Sci. 24, 1853. https://doi.org/10.3390/ijms24031853.

Zhang, C., Li, C., Liu, K., Zhang, Y., 2022. Characterization of zearalenone-induced hepatotoxicity and its mechanisms by transcriptomics in zebrafish model. Chemosphere 309, 136637. https://doi.org/10.1016/j.chemosphere.2022.136637.

Zhang, Q., Xia, R., Shao, J., Ren, R., Sun, Y., Zhang, Y., Wang, F., Zhang, G., 2025. Zearalenone regulates energy metabolism and proliferation of Goat endometrial epithelial cells through Estrogen receptor 1. J. Agric. Food Chem. 73, 20385–20395. https://doi.org/10.1021/acs.jafc.5c05264.

Zhang, T.Y., Suen, C.Y., 1984. A fast parallel algorithm for thinning digital patterns. Commun. ACM 27, 236–239.

Zhang, W., Zhang, S., Zhang, M., Yang, L., Cheng, B., Li, J., Shan, A., 2018. Individual and combined effects of Fusarium toxins on apoptosis in PK15 cells and the protective role of N-acetylcysteine. Food Chem. Toxicol. 111, 27–43. https://doi.org/10.1016/j.fct.2017.10.057.

Zhao, L., Xiao, Y., Li, C., Zhang, J., Zhang, Y., Wu, M., Ma, T., Yang, L., Wang, X., Jiang, H., Li, Q., Zhao, H., Wang, Y., Wang, A., Jin, Y., Chen, H., 2021. Zearalenone perturbs the circadian clock and inhibits testosterone synthesis in mouse Leydig cells. J. Toxicol. Environ. Health 84, 112–124. https://doi.org/10.1080/15287394.2020.1841699.

Zheng, W., Huang, Q., Pan, S., Fan, W., Wang, G., Yuan, Y., Gu, J., Liu, X., Liu, Z., Bian, J., 2017. Regulation of oncogenes and gap junction intercellular communication during the proliferative response of zearalenone in TM3 cells. Hum. Exp. Toxicol. 36, 701–708. https://doi.org/10.1177/0960327116661021.

Zheng, W., Wang, B., Li, X., Wang, T., Zou, H., Gu, J., Yuan, Y., Liu, X., Bai, J., Bian, J., Liu, Z., 2018a. Zearalenone promotes cell proliferation or causes cell death? Toxins 10, 184.

Zheng, W., Wang, B., Si, M., Zou, H., Song, R., Gu, J., Yuan, Y., Liu, X., Zhu, G., Bai, J., Bian, J., Liu, Z., 2018b. Zearalenone altered the cytoskeletal structure via ER stress-autophagy- oxidative stress pathway in mouse TM4 Sertoli cells. Sci. Rep. 8, 3320. https://doi.org/10.1038/s41598-018-21567-8.

Zhou, H., George, S., Hay, C., Lee, J., Qian, H., Sun, X., 2017. Individual and combined effects of Aflatoxin B1, Deoxynivalenol and Zearalenone on HepG2 and RAW 264.7 cell lines. Food Chem. Toxicol. 103, 18–27. https://doi.org/10.1016/j.fct.2017.02.017.

Zhu, D., Li, Y., Liu, M., Yang, Y., Fu, J., Su, L., Wang, F., Cen, Y., Zhou, Y., Li, Y., 2025. Study on the role of mitophagy and pyroptosis induced by nano-silver in testicular injury. Food Chem. Toxicol. 197, 115245. https://doi.org/10.1016/j.fct.2025.115245.

Zinedine, A., Soriano, J.M., Moltó, J.C., Mañes, J., 2007. Review on the toxicity, Occurrence, Metabolism, Detoxification, Regulations and Intake of Zearalenone: an oestrogenic mycotoxin. Food Chem. Toxicol. 45, 1–18. https://doi.org/10.1016/j.fct.2006.07.030.

Zirkin, B.R., Papadopoulos, V., 2018. Leydig cells: formation, Function, and regulation. Biol. Reprod. 99, 101–111. https://doi.org/10.1093/biolre/ioy059.